catalysts

MDPI

Article

Quantitative Structure-Thermostability Relationship of Late Transition Metal Catalysts in Ethylene Oligo/Polymerization

Wenhong Yang [1,2,*], Zhifeng Ma [1,2], Jun Yi [1,2] and Wen-Hua Sun [1,2,*]

1 Key Laboratory of Engineering Plastics and Beijing National Laboratory for Molecular Science, Institute of Chemistry, Chinese Academy of Sciences, Beijing 100190, China; mazhifeng@iccas.ac.cn (Z.M.); yijunacs@iccas.ac.cn (J.Y.)

2 University of Chinese Academy of Sciences, Beijing 100049, China

* Correspondence: whyang@iccas.ac.cn (W.Y.); whsun@iccas.ac.cn (W.-H.S.); Tel.: +86-10-6255-7955 (W.Y. & W.-H.S.)

Academic Editor: José R. B. Gomes
Received: 23 February 2017; Accepted: 14 April 2017; Published: 18 April 2017

Abstract: Quantitative structure–thermostability relationship was carried out for four series of bis(imino)pyridine iron (cobalt) complexes and α-diimine nickel complexes systems in ethylene oligo/polymerization. Three structural parameters were correlated with thermal stability, including bond order of metal-nitrogen (B), minimum distance (D) between central metal and *ortho*-carbon atoms on the aryl moiety and dihedral angle (α) of a central five-membered ring. The variation degree of catalytic activities between optimum and room temperatures (A_T) was calculated to describe the thermal stability of the complex. By multiple linear regression analysis (MLRA), the thermal stability presents good correlation with three structural parameters with the correlation coefficients (R^2) over 0.95. Furthermore, the contributions of each parameter were evaluated. Through this work, it is expected to help the design of a late transition metal complex with thermal stability at the molecular level.

Keywords: structure–thermostability relationship; late transition metal complex; homogeneous catalysis; ethylene polymerization; molecular modeling

1. Introduction

Since the discovery of nickel and palladium catalysts bearing α-diimine ligands, the growth of late transition metal complex catalysts for ethylene reactivity has been promoted due to their particular features, such as stable structure, low cost and high catalytic activities in the polymerization of ethylene [1–6]. In order to get desirable catalytic performance, extensive achievement and progress have been obtained through modifying substituents of used ligands and designing alternative ligands as well as optimizing reaction conditions [7–18]. However, in large-scale polymerizations, the exothermic property of the polymerization reaction deactivates the catalysts by the quick decomposition and β-H elimination at elevated bulk reaction temperature [19–22], greatly hindering the potential development in the field of industrial applications [23].

To improve the thermal stability of a catalyst, tremendous experimental works were conducted and significant progress achieved. Guan et al. early reported a series of novel nickel catalysts bearing the cyclophane ligands (Scheme 1, **A**) and phosphine imine hybrid ligands (Scheme 1, **B**), which revealed high activities at high temperatures for ethylene polymerization. The complex **A** presents a turnover frequency (TOF) of 1.0×10^6 h^{-1} at 90 °C and complex B shows a TOF of 1.7×10^4 h^{-1} at 70 °C [24–26]. Subsequently, the camphyl-based nickel catalysts (Scheme 1, **C**) exhibited good thermal

stability; meanwhile, the obtained polymer had a significant narrow molecular weight distribution (polydispersity index: PDI < 1.2) [27,28]. The Long group also reported a robust nickel α-diimine catalyst (Scheme 1, **D**) for ethylene polymerization at a high temperature. The TOF maintains about 1.0×10^5 h^{-1} at 100 °C. Moreover, the observed molecular weight distribution of the polyethylene is still very narrow (about 1.25) at such a high temperature [29]. In addition, our group reported the nickel complex catalysts containing acenaphthylene ligands (Scheme 1, **E**), which showed high catalytic activities (10^6 g·mol^{-1}(Ni)·h^{-1}) and high molecular weight of the produced polyethylene (10^6 g·mol^{-1}) at temperature of 80 °C [30]. In addition, the iron-based complex catalysts bearing bis(imino)pyridine ligands with bulky substituents (Scheme 1, **F**) exhibited good thermal stability with catalytic activities of 10^6 g·mol^{-1}(Fe)·h^{-1} at 60–80 °C [31–37].

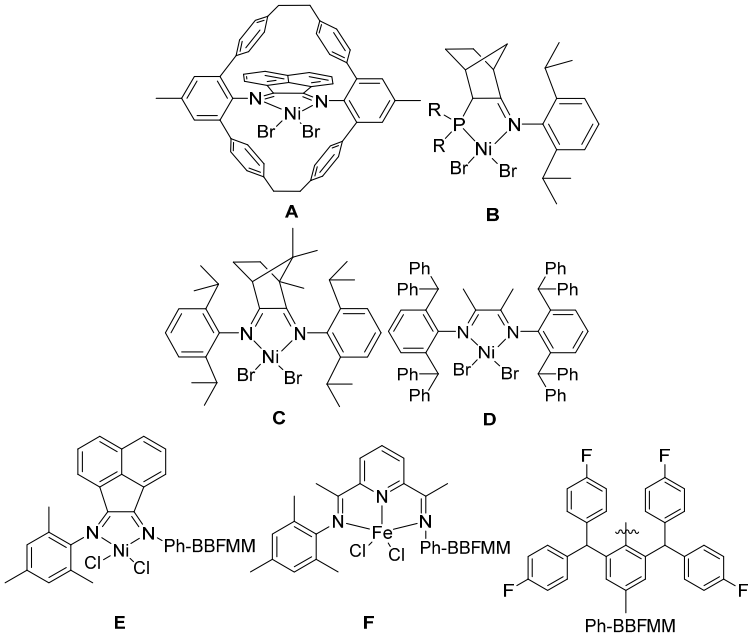

Scheme 1. The structures of the nickel and iron complexes with thermal stability.

In the complexity of the whole polymerization process, the underlying reasons for the observed changes of catalytic activities are often unclear, but there is no doubt that catalyst structures play a key role in determination of catalytic activities. As a result, the quantitative structure–property relationship (QSPR) approach has proven to be useful. In our previous studies, the relationship between the structure of a catalyst and its catalytic activity was investigated by molecular modeling, which successfully predicted the catalytic activities of late transition metal complex precatalysts toward ethylene oligo/polymerization, through electronic effects [38–41] or both from electronic and steric effects [42,43]. Regarding the influence of the catalyst structure on its thermal stability, several possible factors were proposed by previous experimental research [19,24–26,29–36]. However, to our best knowledge, there are less detailed works at a molecular level to study the catalyst with thermal stability quantitatively.

Herein, detailed works on this topic at a molecular level were performed to explain the essential mechanism of the catalyst with thermal stability quantitatively. Three structural parameters were defined and calculated to correlate with the thermal stability for four series of typical late transition metal complexes from our previous reports [30–36,44–47]. The results showed that a catalyst's thermal stability has very good relationships with three structural parameters by using multiple linear regression analysis (MLRA). The obtained correlation coefficient values of R^2 are over 0.949. By analyzing the contribution of each parameter, the main effect on thermal stability regarding different frameworks of precatalysts was proposed.

2. Results and Discussion

2.1. Definition of the Parameters Related to Thermal Stability

In the present work, three parameters were chosen to characterize the thermal stability of late transition metal complex, including the bond order (B), minimum distance (D) and dihedral angle (α). Regarding bond order (B), it represents the strength of the bond between metal atoms and coordinated heteroatoms within ligands, which are nitrogen atoms for the modeled complexes. The bond strength of metal and nitrogen atoms (M–N) should be strong enough to prevent them from breaking (or decomposition) at high temperatures [26]. Since there are usually two or three M–N bonds, the minimum value of bond order (B) was chosen. According to previous research, the formation of the five- or six-membered metallacycle via intramolecular C–H activation demonstrated in Scheme 2 may deactivate the catalyst, reducing the thermal stability of a catalyst [19]. Therefore, the minimum distance (D) between central metal and carbon atoms highlighted in blue (M–C) was calculated. The parameter α is the dihedral angle of the central five-membered ring shown in the Scheme 2 with the atoms in red. This factor indicates the stability of the complex due to the stress and strain of the central five-membered ring within a catalyst [48]. For an NˆNˆN three chelated complex, the value of α is the average data for two central five-membered rings.

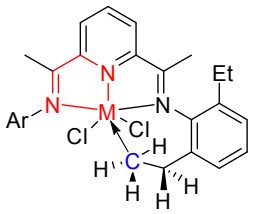

Scheme 2. The description of minimum distance (D) and central five-membered ring.

To measure the thermal stability of different complexes, the variation values of catalytic activities at different reaction temperatures (A_T) were calculated by Equation (1):

$$A_T = \frac{A_{opt} - A_r}{A_r} \quad (1)$$

where A_{opt} and A_r are the activities at optimum and room temperatures for each complex, respectively. Most of the model complexes in this work were taken from our previous experimental results, and the detailed values of activities at both optimum and room temperatures were provided in Table S1 of Supplementary Materials.

The calculated parameters (B, D, α) were related to the A_T by the MLRA Equation (2), which was resolved by the regression analysis based on the least squares method in Microsoft Excel [49]. After fitting, the values of x_0, x_1, x_2 and x_3 were automatically obtained:

$$A_T = x_0 + x_1 B + x_2 D + x_3 \quad (2)$$

In order to analyze the contribution of each parameter to the thermal stability for each complex system, the values of B, D and α were standardized using the Z-Score method. Then, the contribution was calculated by the Equation (3) based on our previous works:

$$Contribution(\%) = \frac{\sum_{j=1}^{j=n} \frac{|x_i m_{ij}|}{\sum_{1}^{i=3} |x_i m_{ij}|}}{n} \times 100\% \quad (3)$$

where i is the serial number of parameter, j is the order of the complex, m_{ij} is the value of each parameter for each complex, x_i is the regression coefficient of each parameter, and n is the total number of complexes.

2.2. Thermal Stability of Bis(imino)pyridyliron(cobalt) Complexes

The main framework of the catalyst with thermal stability can be classified into two categories including the bis(imino)pyridyliron(cobalt) and the α-diiminenickel complexes. In this section, the bis(imino)pyridyliron(cobalt) complexes **1**–**10** as showed in the Schemes 3 and 4 from previous reports [31–36] were selected to study the thermal stability. For the complexes **1**–**5**, the small variations of structures lie in the different substituents within the aryl moiety, while, for the complexes **6**–**10**, the differences are not only the substituents within the aryl moiety, but also the A_r group. Furthermore, the experimental conditions were totally the same for complexes **1**–**5**, while, for complexes **6**–**10**, there was little difference. Therefore, the complexes were divided into two systems: complexes **1**–**5** and complexes **6**–**10**.

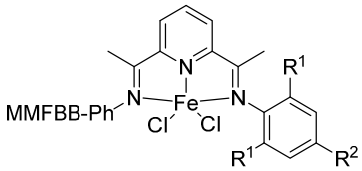

	1	2	3	4	5
R^1	Me	Et	*i*-Pr	Me	Et
R^2	H	H	H	Me	Me

Scheme 3. The structures of bis(imino)pyridyliron complexes **1**–**5**.

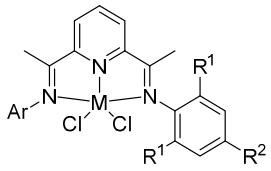

	6	7	8	9	10
Ar	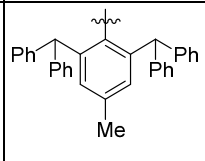	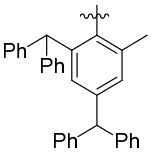	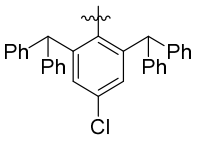	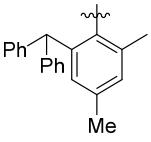	Ph-BBFMM
R^1	*i*-Pr	Et	Me	*i*-Pr	Me
R^2	H	Me	Me	H	Me
M	Fe	Fe	Fe	Fe	Co

Scheme 4. The structures of bis(imino)pyridyliron(cobalt) complexes **6**–**10**.

In this study, the calculated three parameters (B, D, α) are heavily dependent on the geometry structure, so the optimization of the complex structure was performed by the molecular mechanics (MM) method. The comparisons between calculated structure and experimental crystal data for the selected bond lengths and bond angles for complexes **1**, **5** and **7** were listed in Table 1. It is clearly seen that the values of standard deviation δ for all three of these complexes are very small, indicating the reasonableness of the optimized structures. This guarantees a reliable relationship between structure parameters (B, D, α) and the thermal stability.

Table 1. The calculated bond lengths and bond angles compared with experimental crystal structures for complexes **1**, **5**, and **7** along with the values of standard deviation δ. MM, molecular mechanics.

Bond	Bond Lengths (Å)					
	Complex 1		Complex 5		Complex 7	
	X-ray	MM	X-ray	MM	X-ray	MM
Fe–N1	2.228	2.201	2.201	2.195	2.278	2.239
Fe–N2	2.061	2.072	2.057	2.061	2.111	2.118
Fe–N3	2.178	2.195	2.157	2.196	2.268	2.236
Fe–Cl1	2.319	2.319	2.298	2.298	2.290	2.290
Fe–Cl2	2.264	2.264	2.252	2.252	2.290	2.289
δ	-	0.768	-	0.834	-	0.925
Angle	**Bond Angles (°)**					
	Complex 1		Complex 5		Complex 7	
	X-ray	MM	X-ray	MM	X-ray	MM
N1–Fe–N2	72.80	73.33	73.21	73.29	72.52	73.64
N2–Fe–N3	74.02	73.54	74.51	73.51	73.92	73.56
N1–Fe–N3	141.12	143.32	142.21	142.56	146.42	146.21
N1–Fe–Cl1	101.72	98.40	101.35	99.09	96.81	97.77
N2–Fe–Cl1	91.72	92.67	92.33	92.33	121.41	121.32
N3–Fe–Cl1	99.02	98.43	99.10	99.07	101.11	98.79
N1–Fe–Cl2	98.72	100.47	96.68	100.18	98.51	100.62
N2–Fe–Cl2	151.10	150.26	151.60	150.52	122.61	121.12
N3–Fe–Cl2	100.62	100.45	102.45	100.17	98.81	97.02
Cl1–Fe–Cl2	117.19	117.07	115.89	117.16	155.95	154.65
δ	-	1.45	-	1.71	-	1.43

Accordingly, the three structural parameters calculated were obtained and listed in Table 2 for complexes **1**–**5**. Clearly, the variations of the three parameters as a function of substituents were very small. Regarding the bond order (*B*), the values are from 0.1028 to 0.1048, meaning that there is little change in bond strength between iron and nitrogen with various substituents. For the minimum distance parameter (*D*), all of the calculated results were above 2.0 Å, indicating no formation of an inter M–C bond, which improves the thermal stability of complex. As for a dihedral angle (α), it is shown in Table 2 that the obtained values of α were from 7.839° to 8.627°. From previous study, it is indicated that the half-chair configuration (non plane form) of the central five-membered ring is helpful for the stability of the complex [46]. Therefore, the bigger the value of α, the more stable the complex is.

Table 2. The original and standardized values of bond order (*B*), minimum distance (*D*) and dihedral angle (α) for complexes **1**–**5**.

Original Values				
Complex	***B***	***D* (Å)**	**α (°)**	A_T
1	0.1048	2.427	7.839	5.313
2	0.1048	2.073	8.245	5.689
3	0.1028	2.293	8.206	7.710
4	0.1042	2.221	8.259	6.333
5	0.1048	2.147	8.627	4.082
Standardized Values				
Complex	***B***	***D* (Å)**	**α (°)**	A_T
1	0.5996	1.4286	−1.4173	−0.3838
2	0.5996	−1.1675	0.0347	−0.1022
3	−1.7067	0.4459	−0.1049	1.4116
4	−0.0923	−0.0821	0.0831	0.3802
5	0.2996	−0.6248	1.4044	−1.3058

To quantitatively analyze the influence of catalyst structure on thermal stability, the relationship between B, D, α and A_T was fitted using the multiple linear regression Equation (2). The regression and correlation coefficient values were obtained and listed in Table 3. Then, the thermal stabilities were calculated by the fitting equation and compared with experimental results for the complexes **1–5**. The result shows that almost all points were in a diagonal line in Figure 1a, suggesting that the calculated and experimental A_T values are very close. The obtained correlation coefficient value (R^2) is 0.970.

Table 3. The original and standardized regression coefficients (x) values of multiple linear regression equation as well as correlation coefficients (R^2) for the complexes. Or., original; St., standardized .

Complexes	Type	x_0	x_1	x_2	x_3	R^2
Complexes **1–5**	Or.	199.46	−1493.89	−4.909	−3.266	0.970
	St.	-1.0×10^{-14}	−0.970	−0.501	−0.683	-
Complexes **6–10**	Or.	−33.32	197.02	5.149	0.536	0.949
	St.	-2.3×10^{-16}	1.081	0.616	0.438	-
Complexes **11–15**	Or.	458.54	−7450.7	33.59	25.84	0.998
	St.	-6.1×10^{-16}	−0.244	0.110	1.002	-
Complexes **16–20**	Or.	2.344	−32.898	0.609	0.039	0.998
	St.	-1.9×10^{-16}	−0.935	0.351	0.166	-

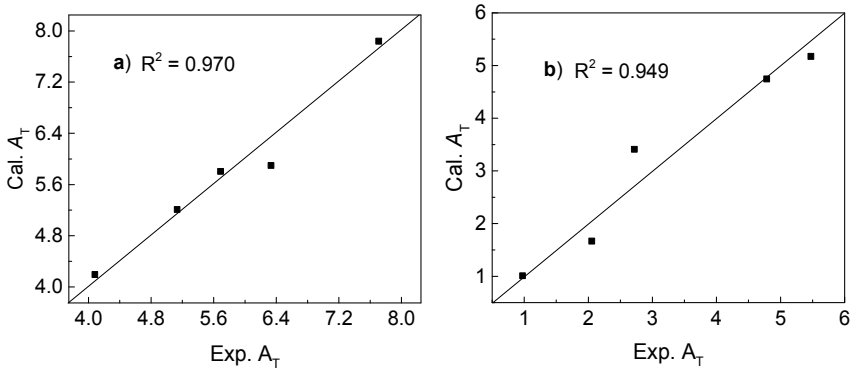

Figure 1. The plots of calculated value of thermal stability (Cal. A_T) versus experimental results (Exp. A_T) for complexes **1–5** (**a**) and complexes **6–10** (**b**).

In the same manner, for complexes **6–10**, three parameters were obtained and listed in Table 4. For bond order (B), the calculated values were in the range of 0.0788 to 0.1031, which were smaller compared with the results of complexes **1–5** (Table 2), especially for complex **10**, signifying the potential reduction of their thermal stabilities. For the minimum distance (D), all of the data were over 2.00 Å, indicating that no metallacycle ring formed either. Regarding the dihedral angle (α), the results ranged from 7.335° to 11.413°. From the variation of the structure parameters, the thermal stabilities of complexes **6–10** should be lower than that of complexes **1–5**. For clarity, the averaged values of the catalytic activities for complexes **1–5** and **6–10** were plotted in Figure 2 at room and optimum temperatures. Obviously, the thermal stability of the former is better than the latter, although the catalytic activities at room temperature are almost the same.

Table 4. The original and standardized values of bond order (*B*), minimum distance (*D*) and dihedral angle (*α*) for complexes **6**–**10**.

Original Values				
Complex	***B***	***D* (Å)**	***α* (°)**	A_T
6	0.1019	2.383	8.187	2.719
7	0.1026	2.280	11.413	4.784
8	0.1031	2.607	8.885	5.474
9	0.0987	2.256	7.335	2.054
10	0.0788	2.778	8.409	0.974
Standardized Values				
Complex	***B***	***D* (Å)**	***α* (°)**	A_T
6	0.4725	−0.3456	−0.4275	−0.2560
7	0.5402	−0.8032	1.6695	0.8408
8	0.5887	0.6495	0.0254	1.2072
9	0.1626	−0.9098	−0.9803	−0.6092
10	−1.7641	1.4092	−0.2835	−1.1828

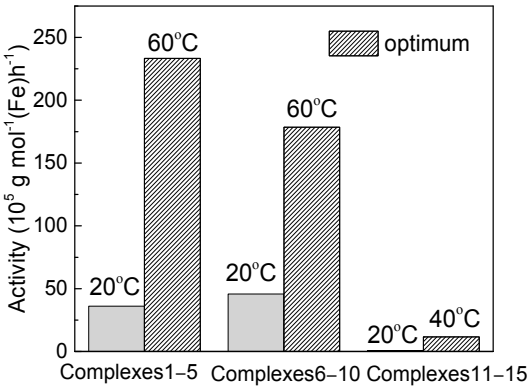

Figure 2. Comparisons of the average catalytic activities for complexes **1**–**5**, **6**–**10** and complexes **11**–**15** at room and optimum temperatures, respectively.

Accordingly, from the values of A_T in Tables 2 and 4, the thermal stabilities of complexes **6**–**10** are lower than that of complexes **1**–**5** correspondingly. This result is in agreement with the decrease of bond order (*B*), suggesting that this parameter has an outstanding influence on the thermal stability of this series of complex system. By the MLRA method, the regression coefficients were obtained and showed in Table 3. Then, the calculated values of thermal stabilities were obtained and compared with experimental results, which present good correlation with the R^2 value of 0.949 as showed in Figure 1b.

In order to quantitatively investigate the influence of each parameter on the thermal stability, the values of three parameters and thermal stabilities were further standardized by the *Z*-Score method. The obtained values of the *B*, *D*, *α*, A_T were collected in Tables 2 and 4 for complexes **1**–**5** and complexes **6**–**10**, respectively, and the corresponding standard regression coefficients were obtained and listed in Table 3. Then, using Equation (3), the contributions of each parameter were calculated. The obtained contribution values of the *B*, *D* and *α* for the complexes **1**–**5** are 48%, 26% and 26%, respectively. Therefore, it indicates that the bond order dominates the thermal stabilities of complexes **1**–**5**. Similarly, the contributions of the *B*, *D* and *α* for the complexes **6**–**10** are calculated and the results are 46%, 33% and 21%, respectively. It suggests that the bond order plays a predominant role in determining the thermal stabilities for complexes **6**–**10** as well.

2.3. Thermal Stability of Phenanthrolinyliron Complexes

For the derivatives of bis(imino)pyridyline, the phenanthrolinyliron complexes also showed good thermal stability. Here, we selected a series of complexes **11–15** from our previous reports [47] with the structures showed in the Scheme 5. In the same manner, the values of bond order (B), minimum distance (D) and dihedral angle (α) as well as the results of the thermal stabilities (A_T), accordingly, were obtained and listed in Table 5.

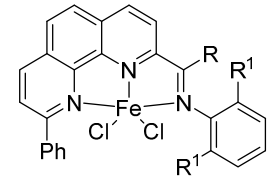

	11	12	13	14	15
R^1	Me	Et	*i*-Pr	Me	Et
R	Me	Me	Me	Ph	Ph

Scheme 5. The structures of phenanthrolinyliron complexes **11–15**.

Table 5. The original and standardized values of bond order (B), minimum distance (D) and dihedral angle (α) along with thermal stability (A_T) for complexes **11–15**, respectively.

Original Values				
Complex	***B***	***D* (Å)**	**α (°)**	A_T
11	0.0770	3.677	1.815	55.276
12	0.0786	3.624	1.309	28.386
13	0.0769	3.522	0.189	8.548
14	0.0774	3.689	0.093	6.992
15	0.0774	3.660	0.132	9.585
Standardized Values				
Complex	***B***	***D* (Å)**	**α (°)**	A_T
11	−0.6797	0.6317	1.3825	1.622
12	1.6845	−0.1542	0.7510	0.321
13	−0.8275	−1.6666	−0.6467	−0.639
14	−0.0887	0.8096	−0.7677	−0.714
15	−0.0887	0.3796	−0.7191	−0.589

Compared with complexes **1–10**, the values of bond order (B) and dihedral angle (α) of complexes **11–15** decreased obviously. To see the variation of the catalytic activities from experiments, the average values at room temperature and optimum temperature were showed in Figure 2 for complexes **11–15**. It is clear that the average activities and thermal stabilities of complexes **11–15** are obviously lower than that of complexes **1–5** and **6–10**. These observations are in agreement with the decrease values of the calculated bond order (B) and dihedral angle (α) values within complexes **11–15**. On another side, the values of thermal stability (A_T) for complexes **11–15** are large, as showed in Table 5, especially for complexes **11** and **12**. This can be explained by the very low catalytic activities at room temperature.

Then, the regression coefficients of fitting equation were calculated, and the values were listed in Table 3. Comparison of calculated and experimental A_T was conducted as showed in Figure 3. Obviously, there is a good correlation with the coefficient (R^2) value of 0.998, meaning that the thermal stabilities of complexes **11–15** were reasonably investigated.

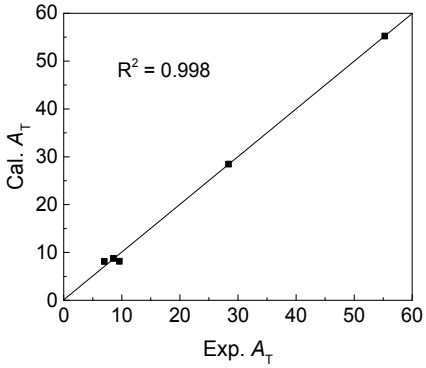

Figure 3. The plots of calculated thermal stabilities (Cal. A_T) versus experimental results (Exp. A_T) for complexes **11**–**15**.

To further analyze the influence of each parameter on thermal stability, the B, D, α and A_T values were standardized and the results were collected in Table 5. Based on the standardized fitting equation, the contributions of each parameter were calculated accordingly. The obtained contribution of the dihedral angle (α) is 78%, whereas those of bond order (B) and minimum distance (D) are 14% and 8%, respectively. These results reveal that, different from complexes **1**–**5** and **6**–**10**, the dihedral angle became the major factor to determine the thermal stabilities of complexes **11**–**15**.

2.4. Thermal Stability of Acenaphthylnickel Complexes

As discussed in the introduction, besides the framework of bis(imino)pyridyline complex, the system with an acenaphthylene backbone also shows good thermal stability towards ethylene polymerization. In this section, a series of nickel complexes **16**–**20** containing acenaphthylene ligands [30,43–46] were investigated regarding the property of thermal stability. The structures of model complexes were showed in the Scheme 6.

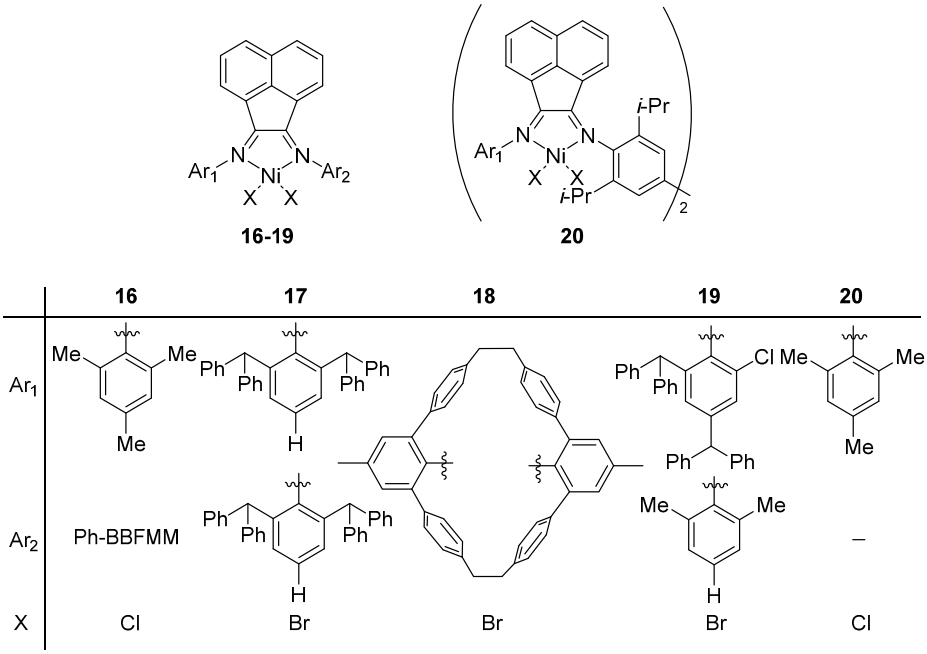

Scheme 6. The structures of the acenaphthylnickel complexes **16**–**20**.

By the same method, three parameters (B, D, α) were firstly obtained and listed in Table 6 along with the values of thermal stabilities (A_T) for each complex. By the regression analysis method, the regression coefficients were obtained and showed in Table 3. Then, the thermal stabilities were calculated and compared with experimental data. Results revealed in Figure 4 that calculation values are in very agreement with experiments with the correlation coefficient (R^2) value of 0.998.

Table 6. The original and standardized values of bond order (B), minimum distance (D) and dihedral angle (α) along with thermal stability (A_T) for complexes **16**–**20**, respectively.

Original Values				
Complex	***B***	***D* (Å)**	**α (°)**	A_T
16	0.1114	2.671	0.207	0.337
17	0.0993	2.626	4.245	0.845
18	0.1017	2.251	1.412	0.414
19	0.0836	2.784	0.139	1.294
20	0.1129	2.873	0.286	0.370
Standardized Values				
Complex	***B***	***D* (Å)**	**α (°)**	A_T
16	0.8183	0.126	−0.601	−0.761
17	−0.2110	−0.063	1.707	0.466
18	−0.0068	−1.635	−0.088	−0.575
19	−1.5464	0.560	−0.639	1.552
20	0.9458	0.973	−0.555	−0.682

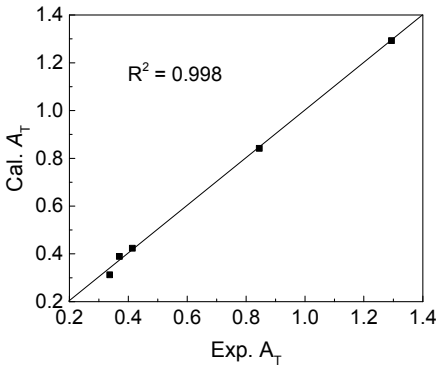

Figure 4. The plot of calculated thermal stability (Cal. A_T) versus experimental thermal stability (Exp. A_T) for complexes **16**–**20**.

Based on standardized values of B, D, α and A_T as well as the corresponding standard regression coefficients in Table 3, the contributions of each factor were calculated accordingly, which showed the values of 49%, 22% and 29% for bond order (B), minimum distance (D) and dihedral angle (α), respectively, signifying the dominant role of bond order in the thermal stabilities of complexes **16**–**20**.

3. Computational Details

Calculation Method for the Parameters

In order to calculate the bond order (B), the structure of complex was firstly optimized by a molecular mechanism (MM) method based on our previous study, which shows that the optimized structures by MM are closer to experimental crystal results [43]. This was performed by the Forcite program package (6.0, Accelrys Inc., San Diego, CA, USA, 2011) using the Dreiding force field due to its capability of reasonable prediction of the structure [50]. However, there are no parameters for late

transition metal elements, such as Fe, Co and Ni, as well as the atom types that connect with metal elements. Therefore, the crystal data of complexes in previous reports [34,45,47], as listed in Table S2 of Supplementary Materials, were added into the file of Dreiding force field. The values of convergence tolerance for the energy and the force were 0.001 and 0.5 kcal·mol^{-1}, respectively. To describe the electrostatic and van der Waals interactions, the atom based Summation and Truncation methods were used, and the cutoff distance of cubic spline was 1.25 nm.

Then, the Mayer bond order was obtained by single point energy calculation by a Gaussian 09 package (C.01, Gaussian, Inc., Wallingford, CT, USA, 2010) using the Natural Bond Orbital (NBO) population [51,52]. Different functional and basis sets may give rise to different bond order results for one structure; therefore, several combinations of parameters were tried as listed in Table 7. From previous research [53], the bond order and bond length should be in accordance with the following Equation (4):

$$B = \exp \frac{[-(R - R_0)R_0]}{a}, \quad (4)$$

where B is bond order, R is the experimental bond length, R_0 is a constant which stands for the equilibrium bond length, and a is also a constant related to the type of bond. Then, the calculated bond orders of three Fe–N bonds for the complex **12** (Scheme 5) and experimental bond lengths were fitted by this equation. The obtained fitting results (R^2) were showed in Table 7. Clearly, the calculation result for bond order using B3LYP/6-31G* [54,55] is better than others. Therefore, this combination of functional and basis set was chosen. As to the dihedral angles (α) for the central five-membered ring, this parameter can be obtained directly from the optimized structure of a complex by MM calculation.

Table 7. The values of bond order (B) by different functional and basis sets and correlation results (R^2) with bond lengths (R) from experiments.

Bond	Bond Order (B)			Bond Length (R)	
	B3LYP/6–31G*	**B3LYP/6–311G****	**BLYP/6–311G****	**BP86/6–311G****	**Experiments**
Fe–N1	0.0768	0.0539	0.0755	0.0761	2.391
Fe–N2	0.1466	0.1154	0.1428	0.1429	2.100
Fe–N3	0.1101	0.0926	0.1228	0.1238	2.298
R^2	0.963	0.524	0.810	0.800	-

With regard to the minimum distance (D), this was calculated by the molecular dynamics (MD) simulation. All of the MD simulations were performed in the ensemble of the constant of atom number, volume and temperature (NVT) using a Dreiding force field implemented in the Material Studio (6.0, Accelrys Inc., 2011). The nonbonded potential truncation was performed by cubic spline with a cutoff distance of 1.25 nm. The electrostatic and van der Waals interactions were treated by an atom based Summation method with a spline width of 0.1 nm. The temperature kept at 300 K by the Berendsen thermostat with a coupling constant of 0.1 ps. Total simulation time was 4 ns with a time step of 1 fs.

To illustrate the rationalization of three parameters in the model, the results of the linear fitting using one, two and three parameters for the bis(imino)pyridyliron (complexes **1**–**5**) and acenaphthylnickel (complexes **16**–**20**) were compared. It can be seen from the results listed in Table S3 of Supplementary Materials that the fitting results with three parameters for two systems are optimum. Therefore, the model with three parameters is used to investigate the thermal stability for late transition metal complexes.

4. Conclusions

The property of thermal stability for late transition metal complex precatalysts is very important for ethylene polymerization, which greatly influences their potential applications in the field of industry. In this work, four series of complexes with thermal stability containing typical structures

were investigated quantitatively by the MLRA method, which was used in our previous studies on the catalytic activities. Based on the proposed mechanism from experimental observation with respect to the thermal stability of a catalyst; herein, three parameters were defined and calculated, including bond order (B), minimum distance (D) and dihedral angle (α). Meanwhile, the parameter (A_T) that calculates the variation degree of catalytic activities between optimum and room temperatures was used to represent the thermal stability of each complex. By the MLRA method, the fitting equations were obtained and the calculated values of thermal stabilities were compared with experimental data. The results show very good correlation with the values of coefficient (R^2) ranged from 0.949 to 0.998, indicating that the thermal stability of a late transition metal complex towards ethylene polymerization can be quantitatively investigated.

Based on standardized values of three parameters (B, D, α), the contributions of each factor to the thermal stability of complex were evaluated accordingly. For the bis(imino)pypridyliron(cobalt) and acenaphthylnickel complexes, the thermal stability was primarily determined by bond order of metal–nitrogen, while for the phenanthrolinyliron complexes, the dihedral angle plays an important role. To the best of our knowledge, these results are the first reported on thermal stability of a late transition metal complex at the molecular level. It is anticipated that the present results can give guidance for experimental design of a late transition metal complex with high activity at high reaction temperatures.

Supplementary Materials: The following are available online at www.mdpi.com/2073-4344/7/4/120/s1, Table S1: The catalytic activities for complexes **1–20** at different temperatures along with the reaction time, Table S2: The bond lengths and bond angles for metal atoms and atoms coordinated with central metal, which were used as parameters of modified Dreiding force field, Table S3: The correlation coefficient (R^2) results for the models of Fe and Ni-based complexes that were fitted by one, two and three parameters, respectively.

Acknowledgments: This work was financially supported by the National Natural Science Foundation of China (Grant Nos. 2124092 and U1362204) and "One-Three-Five" Strategic Planning of Institute of Chemistry Chinese Academy Sciences (ICCAS). The authors also thank the supercomputer resources and software provided by the University of Missouri-Columbia and the Japan Advanced Institute of Science and Technology.

Author Contributions: Wenhong Yang and Wen-Hua Sun conceived and designed the experiments; Zhifeng Ma performed the experiments; Jun Yi contributed analysis tools; and Wenhong Yang, Zhifeng Ma and Wen-Hua Sun analyzed the data and wrote the paper.

Conflicts of Interest: The authors declare no conflicts of Interest.

References

1. Johnson, L.K.; Killian, M.C.; Brookhart, M. New Pd(II)- and Ni(II)-based catalysts for polymerization of ethylene and α-olefins. *J. Am. Chem. Soc.* **1995**, *117*, 6414–6415. [CrossRef]
2. Johnson, L.K.; Mecking, S.; Brookhart, M. Copolymerization of ethylene and propylene with functionalized vinyl monomers by palladium(II) catalysts. *J. Am. Chem. Soc.* **1996**, *118*, 267–268. [CrossRef]
3. Mecking, S.; Johnson, L.K.; Wang, L.; Brookhart, M. Mechanistic studies of the palladium-catalyzed copolymerization of ethylene and α-olefins with methyl acrylate. *J. Am. Chem. Soc.* **1998**, *120*, 888–899. [CrossRef]
4. Ittel, S.D.; Johnson, L.K.; Brookhart, M. Late-metal catalysts for ethylene homo- and copolymerization. *Chem. Rev.* **2000**, *100*, 1169–1203. [CrossRef] [PubMed]
5. Gibson, V.C.; Spitzmesser, S.K. Advances in non-metallocene olefin polymerization catalysis. *Chem. Rev.* **2003**, *103*, 283–315. [CrossRef] [PubMed]
6. Chen, G.; Ma, X.S.; Guan, Z. Synthesis of functional olefin copolymers with controllable topologies using a chain-walking catalyst. *J. Am. Chem. Soc.* **2003**, *125*, 6697–6704. [CrossRef] [PubMed]
7. Younkin, T.R.; Connor, E.F.; Henderson, J.I.; Friedrich, S.K.; Grubbs, R.H.; Bansleben, D.A. Neutral, single component nickel (II) polyolefin catalysts that tolerate heteroatoms. *Science* **2000**, *287*, 460–462. [CrossRef] [PubMed]
8. Hicks, F.A.; Brookhart, M.A. Highly active anilinotropone based neutral nickel(II) catalyst for ethylene polymerization. *Organometallics* **2001**, *20*, 3217–3219. [CrossRef]

9. Drent, E.; van Dijk, R.; van Ginkel, R.; van Oort, B.; Pugh, R.I. Palladium catalysed copolymerisation of ethene with alkylacrylates: Polar comonomer built into the linear polymer chain. *Chem. Commun.* **2002**, *7*, 744–745. [CrossRef]
10. Gottker Schnetmann, I.; Korthals, B.; Mecking, S. Water-soluble salicylaldiminato Ni(II)-methyl complexes: Enhanced dissociative activation for ethylene polymerization with unprecedented nanoparticle formation. *J. Am. Chem. Soc.* **2006**, *128*, 7708–7709. [CrossRef] [PubMed]
11. Luo, S.; Vela, J.; Lief, G.R.; Jordan, R.F. Copolymerization of Ethylene and alkyl vinyl ethers by a (phosphinesulfonate) PdMe catalyst. *J. Am. Chem. Soc.* **2007**, *129*, 8946–8947. [CrossRef] [PubMed]
12. Kochi, T.; Noda, S.; Yoshimura, K.; Nozaki, K. Formation of linear copolymers of ethylene and acrylonitrile catalyzed by phosphine sulfonate palladium complexes. *J. Am. Chem. Soc.* **2007**, *129*, 8948–8949. [CrossRef] [PubMed]
13. Mu, H.; Pan, L.; Song, D.; Li, Y. Neutral nickel catalysts for olefin homo- and copolymerization: relationships between catalyst structures and catalytic properties. *Chem. Rev.* **2015**, *115*, 12091–12137. [CrossRef] [PubMed]
14. Small, B.L.; Brookhart, M.; Bennett, A.M.A. Highly active iron and cobalt catalysts for the polymerization of ethylene. *J. Am. Chem. Soc.* **1998**, *120*, 4049–4050. [CrossRef]
15. Small, B.L.; Brookhart, M. Iron-based catalysts with exceptionally high activities and selectivities for oligomerization of ethylene to linear α-olefins. *J. Am. Chem. Soc.* **1998**, *120*, 7143–7144. [CrossRef]
16. Britovsek, G.J.P.; Bruce, M.; Gibson, V.C.; Kimberley, B.S.; Maddox, P.J.; Mastroianni, S.; McTavish, S.J.; Redshaw, C.; Solan, G.A.; Strömberg, S.; et al. Polymerization catalysts bearing 2,6-bis(imino)pyridyl ligands: Synthesis, structures, and polymerization studies. *J. Am. Chem. Soc.* **1999**, *121*, 8728–8740. [CrossRef]
17. Bianchini, C.; Giambastiani, G.; Rios, I.G.; Mantovani, G.; Meli, A.; Segarra, A.M. Ethylene oligomerization, homopolymerization and copolymerization by iron and cobalt catalysts with 2,6-(bis-organylimino) pyridyl ligands. *Coord. Chem. Rev.* **2006**, *250*, 1391–1418. [CrossRef]
18. Flisak, Z.; Sun, W.-H. Progression of diiminopyridines: From single application to catalytic versatility. *ACS Catal.* **2015**, *5*, 4713–4724. [CrossRef]
19. Tempel, D.J.; Johnson, L.K.; Huff, R.L.; White, P.S.; Brookhart, M. Mechanistic studies of Pd(II)-α-diimine-catalyzed olefin polymerizations. *J. Am. Chem. Soc.* **2000**, *122*, 6686–6700. [CrossRef]
20. Gates, D.P.; Svejda, S.A.; Oñate, E.; Killian, C.M.; Johnson, L.K.; White, P.S.; Brookhart, M. Synthesis of branched polyethylene using (α-diimine) nickel(II) catalysts: Influence of temperature, ethylene pressure, and ligand structure on polymer properties. *Macromolecules* **2000**, *33*, 2320–2334. [CrossRef]
21. Berkefeld, A.; Mecking, S. Deactivation pathways of neutral Ni(II) polymerization catalysts. *J. Am. Chem. Soc.* **2009**, *131*, 1565–1574. [CrossRef] [PubMed]
22. Guo, L.; Gao, H.; Guan, Q.; Hu, H.; Deng, J.; Liu, J.; Liu, F.; Wu, Q. Substituent effects of the backbone in α-diimine palladium catalysts on homo- and copolymerization of ethylene with methyl acrylate. *Organometallics* **2012**, *31*, 6054–6062. [CrossRef]
23. Xie, T.; McAuley, K.B.; Hsu, J.C.C.; Bacon, D.W. Gas phase ethylene polymerization: Production processes, polymer properties and reactor modeling. *Ind. Eng. Chem. Res.* **1994**, *33*, 449–479. [CrossRef]
24. Camacho, D.H.; Salo, E.V.; Ziller, J.W.; Guan, Z. Cyclophane-based highly active late-transition-metal catalysts for ethylene polymerization. *Angew. Chem. Int. Ed.* **2004**, *43*, 1821–1825. [CrossRef] [PubMed]
25. Camacho, D.H.; Guan, Z. Living polymerization of α-olefins at elevated temperatures catalyzed by a highly active and robust cyclophane-based nickel catalyst. *Macromolecules* **2005**, *38*, 2544–2546. [CrossRef]
26. Guan, Z.; Marshall, W.J. Synthesis of new phosphine imine ligands and their effects on the thermal stability of late-transition-metal olefin polymerization catalysts. *Organometallics* **2002**, *21*, 3580–3586. [CrossRef]
27. Liu, F.; Gao, H.; Hu, Z.; Hu, H.; Zhu, F.; Wu, Q. Poly(1-hexene) with long methylene sequences and controlled branches obtained by a thermostable α-diimine nickel catalyst with bulky camphyl backbone. *J. Polym. Sci. Part A* **2012**, *50*, 3859–3866. [CrossRef]
28. Liu, J.; Chen, D.; Wu, H.; Xiao, Z.; Gao, H.; Zhu, F.; Wu, Q. Polymerization of α-olefins using a camphyl α-diimine nickel catalyst at elevated temperature. *Macromolecules* **2014**, *47*, 3325–3331. [CrossRef]
29. Rhinehart, J.L.; Brown, L.A.; Long, B.K. A Robust Ni(II) α-diimine catalyst for high temperature ethylene polymerization. *J. Am. Chem. Soc.* **2013**, *135*, 16316–16319. [CrossRef] [PubMed]
30. Du, S.; Kong, S.; Shi, Q.; Mao, J.; Guo, C.; Yi, J.; Liang, T.; Sun, W.-H. Enhancing the activity and thermal stability of nickel complex precatalysts using 1-[2,6-bis(bis(4-fluorophenyl)methyl)-4-methyl phenylimino]-2-aryliminoacenaphthylene derivatives. *Organometallics* **2015**, *34*, 582–590. [CrossRef]

31. Yu, J.; Liu, H.; Zhang, W.; Hao, X.; Sun, W.-H. Access to highly active and thermally stable iron procatalysts using bulky 2-[1-(2,6-dibenzhydryl-4-methylphenylimino)ethyl]-6-[1-(arylimino)ethyl] pyridine ligands. *Chem. Commun.* **2011**, *47*, 3257–3259. [CrossRef] [PubMed]
32. Cao, X.; He, F.; Zhao, W.; Cai, Z.; Hao, X.; Shiono, T.; Redshaw, C.; Sun, W.-H. 2-[1-(2,6-Dibenzhydryl-4-chlorophenylimino)ethyl]-6-[1-(arylimino)ethyl] pyridyliron(II) dichlorides: Synthesis, characterization and ethylene polymerization behaviour. *Polymer* **2012**, *53*, 1870–1880. [CrossRef]
33. Zhao, W.; Yu, J.; Song, S.; Yang, W.; Liu, H.; Hao, X.; Redshaw, C.; Sun, W.-H. Controlling the ethylene polymerization parameters in iron pre-catalysts of the type 2-[1-(2,4-dibenzhydryl-6-methyl phenylimino)ethyl]-6-[1-(arylimino)ethyl] pyridyliron dichloride. *Polymer* **2012**, *53*, 130–137. [CrossRef]
34. Sun, W.-H.; Zhao, W.; Yu, J.; Zhang, W.; Hao, X.; Redshaw, C. Enhancing the activity and thermal stability of iron precatalysts using 2-(1-{2,6-bis[bis(4-fluorophenyl) methyl]-4-methylphenylimino}ethyl) -6-[1-(arylimino)ethyl]pyridines. *Macromol. Chem. Phys.* **2012**, *213*, 1266–1273. [CrossRef]
35. Wang, S.; Li, B.; Liang, T.; Redshaw, C.; Li, Y.; Sun, W.-H. Synthesis, characterization and catalytic behavior toward ethylene of 2-[1-(4,6-dimethyl-2-benzhydrylphenylimino)ethyl]-6-[1-(arylimino)ethyl] -pyridyl metal (iron or cobalt) chlorides. *Dalton Trans.* **2013**, *42*, 9188–9197. [CrossRef] [PubMed]
36. Wang, S.; Zhao, W.; Hao, X.; Li, B.; Redshaw, C.; Li, Y.; Sun, W.-H. 2-(1-{2,6-Bis[bis(4-fluorophenyl)methyl]-4-methylphenylimino}ethyl)-6-[1-(arylimino)ethyl]pyridylcobalt dichlorides: Synthesis, characterization and ethylene polymerization behaviour. *J. Organomet. Chem.* **2013**, *731*, 78–84. [CrossRef]
37. Ma, Z.; Yang, W.; Sun, W.-H. Recent progress on transition metal (Fe, Co, Ni, Ti and V) complex catalysts in olefin polymerization with high thermal stability. *Chin. J. Chem.* **2017**. [CrossRef]
38. Yang, W.; Chen, Y.; Sun, W.-H. Assessing catalytic activities through modeling net charges of iron complex precatalysts. *Macromol. Chem. Phys.* **2014**, *215*, 1810–1817. [CrossRef]
39. Chen, Y.; Yang, W.; Sha, R.; Fu, R.-D.; Sun, W.-H. Correlating net charges and the activity of bis(imino)pyridylcobalt complexes in ethylene polymerization. *Inorg. Chim. Acta* **2014**, *423*, 450–453. [CrossRef]
40. Yang, W.; Yi, J.; Sun, W.-H. Revisiting benzylidenequinolinyl nickel catalysts through the electronic effects on catalytic activity by DFT studies. *Macromol. Chem. Phys.* **2015**, *216*, 1125–1133. [CrossRef]
41. Yang, W.; Chen, Y.; Sun, W.-H. Correlating cobalt net charges with catalytic activities of the 2-(benzimidazolyl)-6-(1-aryliminoethyl)pyridylcobalt complexes toward ethylene polymerization. *Macromol. React. Eng.* **2015**, *9*, 473–479. [CrossRef]
42. Yi, J.; Yang, W.; Sun, W.-H. Quantitative investigation of the electronic and steric influences on ethylene oligo/polymerization by 2-azacyclyl-6-aryliminopyridylmetal (Fe, Co, and Cr) complexes. *Macromol. Chem. Phys.* **2016**, *217*, 757–764. [CrossRef]
43. Yang, W.; Ma, Z.; Sun, W.-H. Modeling study on the catalytic activities of 2-imino-1, 10-phenanthrolinylmetal (Fe, Co, and Ni) precatalysts in ethylene oligomerization. *RSC Adv.* **2016**, *6*, 79335–79342. [CrossRef]
44. Rhinehart, J.L.; Mitchell, N.E.; Long, B.K. Enhancing α-diimine catalysts for high-temperature ethylene polymerization. *ACS Catal.* **2014**, *4*, 2501–2504. [CrossRef]
45. Fan, L.; Yue, E.; Du, S.; Guo, C.-Y.; Hao, X.; Sun, W.-H. Enhancing thermo-stability to ethylene polymerization: Synthesis, characterization and the catalytic behavior of 1-(2,4-dibenzhydryl-6-chlorophenylimino)-2-aryliminoacenaphthylnickel halides. *RSC Adv.* **2015**, *5*, 93274–93282. [CrossRef]
46. Kong, S.; Song, K.; Liang, T.; Guo, C.-Y.; Sun, W.-H.; Redshaw, C. Methylene-bridged bimetallic α-diimino nickel(II) complexes: Synthesis and high efficiency in ethylene polymerization. *Dalton Trans.* **2013**, *25*, 9176–9187. [CrossRef] [PubMed]
47. Jie, S.; Zhang, S.; Sun, W.-H. 2-Arylimino-9-phenyl-1, 10-phenanthrolinyl-iron, -cobalt and -nickel complexes: Synthesis, characterization and ethylene oligomerization behavior. *Eur. J. Inorg. Chem.* **2007**, 5584–5598. [CrossRef]
48. Pan, H.; Zhu, L.; Li, J.; Zang, D.; Fu, Z.; Fan, Z. A Thermal stable α-Diimine palladium catalyst for copolymerization of ethylene with functionalized olefins. *J. Mol. Catal. A* **2014**, *390*, 76–82. [CrossRef]
49. Wang, G. *Excel 2013 of Charting and Data Analysis Skills*; China Youth Publishing House: Beijing, China, 2014.
50. Mayo, S.L.; Olafson, B.D.; Goddard, W.A. Dreiding: A generic force field for molecular simulations. *J. Phys. Chem.* **1990**, *94*, 8897–8909. [CrossRef]
51. Mayer, I. Bond orders and valences: Role of d-orbitals for hyfervlent sulphur. *J. Mol. Struct.* **1989**, *149*, 81–89. [CrossRef]

52. Glendening, E.D.; Landis, C.R.; Weinhold, F. Natural bond orbital methods. *WIREs Comput. Mol. Sci.* **2012**, *2*, 1–42. [CrossRef]
53. Lendvay, G. On the correlation of bond order and bond length. *J. Mol. Struct. (Theochem)* **2000**, *501–502*, 389–393. [CrossRef]
54. Hehre, W.J.; Ditchfield, R.; Pople, J.A. Self-consistent molecular orbital methods. XII. Further Extensions of Gaussian-type basis sets for use in molecular orbital studies of organic molecules. *J. Chem. Phys.* **1972**, *56*, 2257–2261. [CrossRef]
55. Szekeres, Z.S.; Bogár, F.; Ladik, J. B3LYP, BLYP and PBE DFT band structures of the nucleotide base stacks. *J. Quant. Chem.* **2005**, *102*, 422–426. [CrossRef]